Received: October 2024, Accepted: December 2025, Published: December 2025
Digital Object Identifier: https://doi.org/10.34302/CJEE/LRBT6157

ENHANCING ISLANDING DETECTION IN PV-BASED DISTRIBUTED SYSTEMS USING CEEMDAN AND PATTERN RECOGNITION NEURAL NETWORK

Sulayman **KUJABI,** Emmanuel Asuming **FRIMPONG,** Francis Boafo **EFFAH**
Department of Electrical and Electronic Engineering, Kwame Nkrumah University of Science and Technology, Kumasi, Ghana
kujabisaul@yahoo.com

Keywords: **Distributed generation, islanding detection, empirical mode decomposition, pattern recognition neural network, CEEMDAN**.

Abstract: *This paper presents an enhanced and practically validated islanding detection framework for grid-connected solar PV systems, integrating Complete Ensemble Empirical Mode Decomposition with Adaptive Noise (CEEMDAN) and a Pattern Recognition Neural Network (PANN). The method processes negative sequence voltage signals at the Point of Common Coupling (PCC) to extract intrinsic mode functions (IMFs), mitigating mode mixing and improving signal fidelity. Significant IMFs are selected based on their power percentile, and three statistical features—maximum value, standard deviation, and entropy—are extracted and normalized before classification by the PANN. Unlike prior studies, this work extends evaluation to zero-power mismatch scenarios, noisy environments, and load-switching conditions, providing practical validation of real-time detection performance. Simulation results demonstrate a classification accuracy of 98.6% with a detection time of 0.1806 seconds, complying with IEEE 1547 standards. The proposed approach exhibits robust and reliable islanding detection across diverse operating conditions, significantly reducing the non-detection zone (NDZ) and enhancing the safety and reliability of modern distribution systems.*

1. INTRODUCTION

The increasing penetration of solar photovoltaic (PV) systems into modern distribution networks has introduced significant operational and protection challenges. Among these, islanding detection remains one of the most critical issues. Islanding occurs when a portion of

the power system continues to be energized by distributed generators (DGs) after being disconnected from the main utility grid[1],[2]. Failure to detect islanding conditions promptly may compromise personnel safety, damage equipment, and degrade power quality. Therefore, fast and reliable islanding detection mechanisms are essential to ensure compliance with IEEE 1547 standards and maintain grid stability.

Conventional islanding detection methods (IDMs) are generally classified as passive, active, or hybrid approaches. Passive methods monitor electrical parameters such as voltage magnitude, frequency deviation, and harmonic distortion. Although relatively simple and cost-effective, these methods often suffer from large non-detection zones (NDZs), particularly under small power mismatch conditions[3,4]. Active methods introduce controlled perturbations into the system to provoke detectable changes during islanding events. While this approach reduces the NDZ, it may adversely affect power quality and increase implementation complexity[4],[5]. Hybrid methods attempt to combine the advantages of passive and active techniques; however, they still face challenges related to reliability, coordination, and practical deployment[6].

Recent advancements in signal processing and artificial intelligence (AI) have enabled more effective islanding detection. Techniques such as Fourier Transform, Wavelet Transform, Hilbert–Huang Transform (HHT), and Empirical Mode Decomposition (EMD) have improved feature extraction from voltage signals [7],[8],[9]. Similarly, machine learning approaches, including artificial neural networks (ANN), support vector machines (SVM), and pattern recognition neural networks (PANN), have demonstrated high accuracy in classifying islanding events[10], [11], [19], [20],[14]

Among advanced decomposition techniques, Complete Ensemble Empirical Mode Decomposition with Adaptive Noise (CEEMDAN) has emerged as an effective solution to the mode-mixing limitations of classical EMD. By adaptively adding noise and ensuring complete signal reconstruction, CEEMDAN provides more reliable intrinsic mode functions (IMFs) for feature extraction. When combined with intelligent classifiers, CEEMDAN-based frameworks offer strong potential for robust islanding detection.

In our previous study[15], a CEEMDAN–PANN-based islanding detection framework was developed using negative sequence voltage measured at the Point of Common Coupling (PCC). Three statistical features derived from selected IMFs—maximum value, standard deviation, and entropy—were used to train the classifier. That study demonstrated high detection accuracy under standard operating conditions and moderate power mismatch scenarios.

However, several practical aspects were not comprehensively investigated in the earlier work, including:

- Zero-power mismatch conditions, where islanding discrimination becomes particularly challenging;
- Extensive fault resistance variations at different grid locations;
- Large-scale load switching disturbances;

- Detailed cross-validation-based robustness assessment;
- Explicit evaluation of real-time detection performance under noisy measurement conditions.

To address these limitations, the present study extends and strengthens the previously proposed CEEMDAN–PANN framework through expanded simulation scenarios and enhanced validation procedures. Specifically, this paper:

1. Evaluates detection performance under zero-power mismatch, representing the most critical NDZ condition.
2. Incorporates noisy signal environments to assess robustness against measurement disturbances.
3. Analyzes fault cases with resistance values ranging from 1 Ω to 70 Ω at varying distances from the PCC.
4. Examines load switching magnitudes up to 20 MW to ensure reliable discrimination from islanding events.
5. Assesses detection time performance to confirm compliance with IEEE 1547 requirements.

By broadening the validation domain and strengthening performance evaluation, this study enhances the practical applicability and robustness of the CEEMDAN–PANN methodology for real-world PV-based distributed generation systems.

The remainder of this paper presents the system modeling, extended simulation scenarios, signal decomposition and feature extraction methodology, classifier training and validation results, and a comparative performance analysis with existing islanding detection approaches.

2. METHODOLOGY

2.1. CEEMDAN-Based Signal Decomposition

Complete Ensemble Empirical Mode Decomposition with Adaptive Noise (CEEMDAN) is used to decompose the negative sequence voltage signal into Intrinsic Mode Functions (IMFs). CEEMDAN improves upon classical EMD and EEMD by adaptively adding Gaussian noise at each decomposition step, ensuring accurate extraction of IMFs and eliminating mode mixing.

The CEEMDAN decomposition process is as follows[16]:

1. Add white Gaussian noise to the original signal:

$$x_i(t) = x(t) + \varepsilon_0 n_i(t) \tag{1}$$

where, ε_0=0.6 is the noise standard deviation amplitude of the added white noise, $x(t)$: Original signal, $n_i(t)$ is the i-th noisy realization.

2. Extract the first IMF from the noisy signal using EMD and average over 100 realizations:

$$IMF_1(t) = \frac{1}{N}\sum_{i=1}^{N} IMF_{1,i}\,(t) \tag{2}$$

3. Residual Calculation:

$$r_1(t) = x(t) - IMF_1(t) \tag{3}$$

4. Repeat adaptive noise addition and IMF extraction iteratively until the residual becomes monotonic or the maximum number of IMFs is reached:

$$x(t) = \sum_{j=1}^{M} IMF_j(t) + r(t) \tag{4}$$

5. Significant IMFs selection: The power of each IMF is computed as:

$$P_i = \sum_{t=1}^{N}[C_i(t)]^2 \tag{5}$$

IMFs with power above the 90th percentile are selected for feature extraction.

2.2. Feature Extraction and Selection

From each significant IMF, three statistical features are extracted:

1. Maximum value:

$$Maximum = max(IMF)$$

2. Standard deviation:

$$standard\ deviation = \sqrt{\frac{1}{N}\sum_{i=1}^{N}(x_i - \bar{x})^2}$$

3. Entropy:

$$entropy = -\sum_{i=1}^{N} p(x_i)\ log_2\big(p(x_i)\big)$$

where, $p(x_i)$ is the probability of each unique IMF value.

2.3. Feature Normalization

The extracted features are normalized using min-max scaling to ensure uniform magnitude and facilitate PANN training:

$$X_{normalized} = \frac{X - X_{min}}{X_{max} - X_{min}} \quad (6)$$

X_{min} *and* X_{max} are the minimum and maximum values of the feature across the dataset.

2.4. PANN Classifier

The Pattern Recognition Neural Network (PANN) structure in *figure 1* is used for islanding detection. The network consists of:

- **Input layer**: 3 neurons (for max, standard deviation, entropy)
- **Hidden layer**: 3 neurons
- **Output layer**: 1 neuron (0 = non-islanding, 1 = islanding)

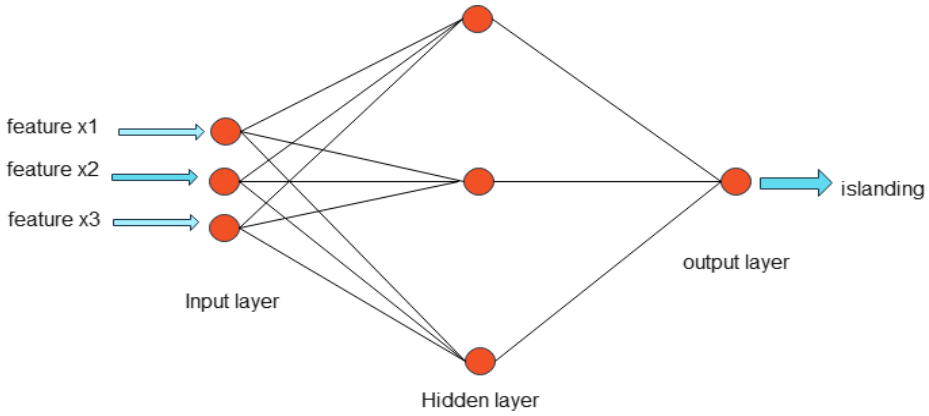

Fig. 1. PANN structure with 3 inputs

The PANN is trained using supervised learning and backpropagation, adjusting weights to minimize prediction errors. The classifier learns patterns and relationships in the features to distinguish islanding from non-islanding events effectively.

2.5. Proposed Detection Algorithm

The overall algorithm is summarized as follows:

1. Acquire negative sequence voltage data from islanding and non-islanding scenarios at the PCC.
2. Add white Gaussian noise (std = 0.6) to enhance decomposition robustness.
3. Apply CEEMDAN across 100 noisy realizations to extract IMFs.

4. Compute IMF power and select significant IMFs (≥90th percentile).
5. Extract max, standard deviation, and entropy from significant IMFs.
6. Normalize the features using min-max scaling.
7. Train the PANN classifier on the extracted features.
8. Classify new voltage signals to detect islanding events.

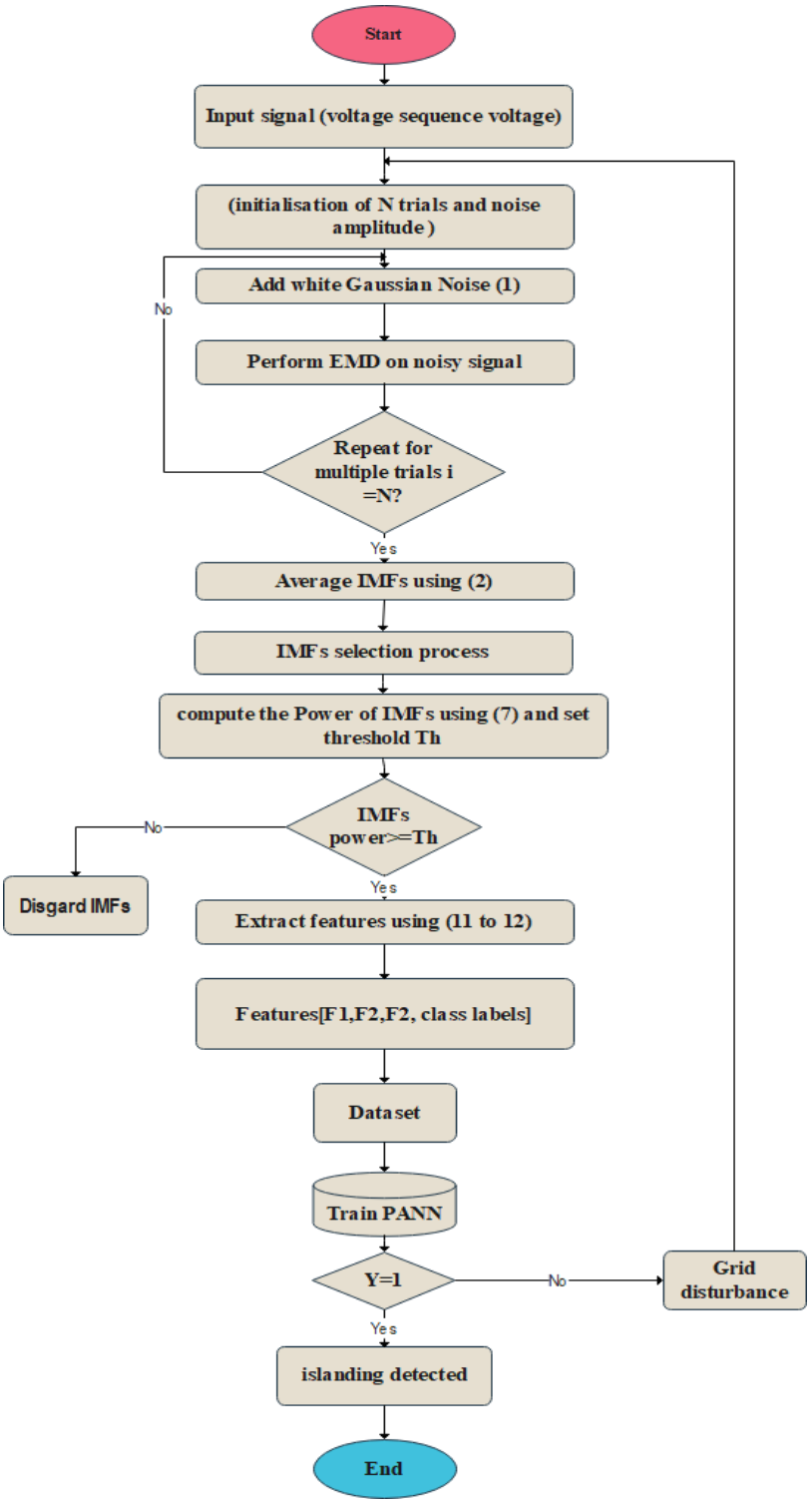

Fig. 2. Flow chart for the proposed islanding detection

Figure 2 illustrates the CEEMDAN–PANN-based islanding detection framework, showing steps from signal acquisition to classification.

3. RESULTS AND DISCUSSION

3.1. Test System for Islanding Detection

The proposed CEEMDAN–PANN islanding detection method was evaluated using a standard test system widely employed in the literature for validating islanding detection algorithms[17],[18]. The system was modeled in MATLAB/Simulink, incorporating realistic grid conditions, distributed solar PV generation, and various load types. *Figure 3* illustrates the studied distributed generation system.

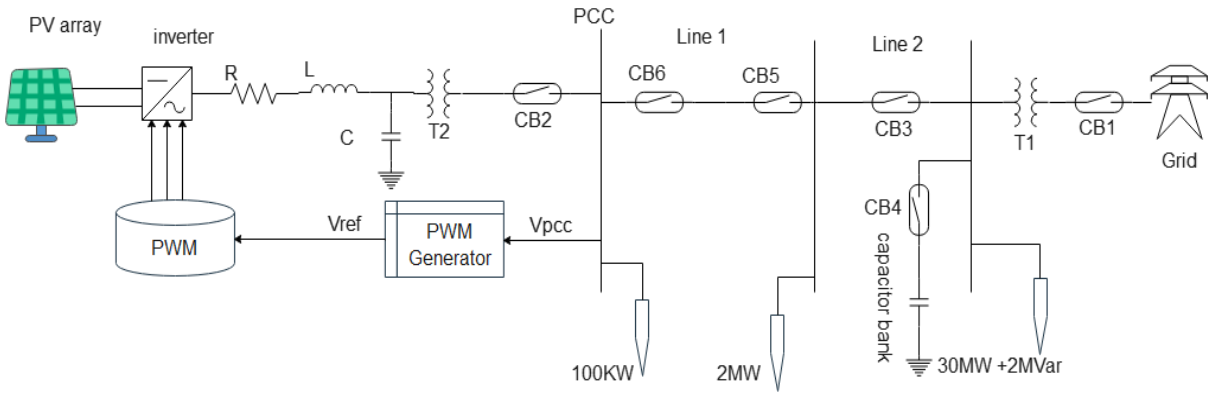

Fig. 3: The studied distributed power generation system

Key components of the system include:

- ✓ **PV-DG unit**: Represents solar photovoltaic generation connected to the grid.
- ✓ **Loads**: Both local and grid-connected loads of varying magnitude and characteristics.
- ✓ **Utility grid and circuit breakers**: Enable simulation of disconnection events and islanding conditions.
- ✓ **Point of Common Coupling (PCC):** Location where negative sequence voltage is measured for monitoring and analysis.

A total of 294 distinct disturbance scenarios were simulated (Table 1), encompassing islanding, fault, and load-switching conditions. The negative sequence voltage was recorded at a sampling frequency of 3.84 kHz over 2.5 s, capturing both transient and steady-state characteristics necessary for robust islanding detection.

Table 1 Simulated grid disturbances

labels	scenarios	Scenarios description	Number of tests
C1	islanding	Tripping circuit breaker during different power mismatch	144
C2	Non islanding	Fault events for 3-phase, 2-phase and single phase	132
C3	Non islanding	Switching of local and grid loads	18

Name of system parameters	Specifications
PV system	Module: sun-power Module model: SunPower SPR-305E-WHT-D Modules in series: 5 No of parallel string: 66 parallel strings PV power rating: 100.7kw Reference voltage: 500V DC Inverter nominal frequency: 60Hz Frequency of the PWM carrier: 33x60Hz Voltage integral and proportional gain: *Ki*:800, *Kp*:7 Current integral and proportional gain: *Ki*:20, *Kp*:0.3
Electric power grid	Rating: 120Kv, and 2500MVA
Transmission line	Resistance: R=0.413 Inductance: L=3.32x10^{-3}H Capacitance: C=5.01x10^{-9}F Rating: *L1*=100kW, *L2*=2MW, *L3*= 30MW+j2MVAr Line voltage: 25KV Length of the line: line-1 is 14km, and line-2 is 5km
Transformer	Voltage level:120kV/25kV Rating: 47MVA for T1, 100kVA, 25kV/0.67kV for T2

3.2. Islanding Scenario (C1)

Islanding events were simulated by tripping the grid-side circuit breaker. *Figure 4* illustrates islanding of the negative sequence voltage response during various power mismatch conditions.

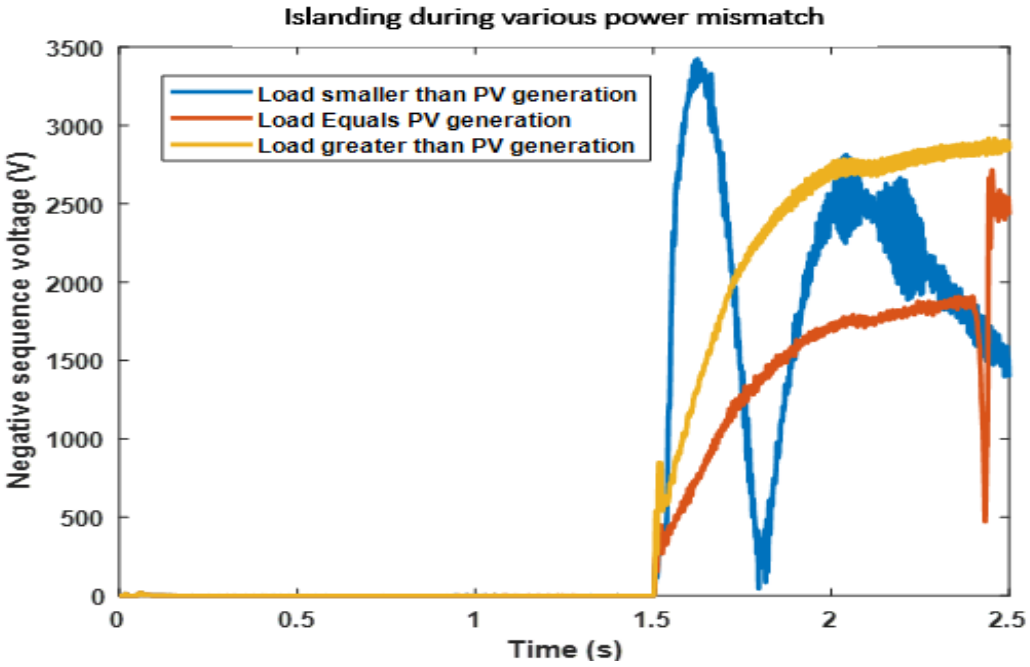

Fig. 4. Islanding during various power mismatch

Under zero-power mismatch, the signal and its IMFs (*Figure 5*) exhibit minimal variation, making differentiation from other disturbances challenging. Three IMFs were extracted:

- ✓ IMF1: Highest frequency content, capturing rapid transient changes.
- ✓ IMF2 & IMF3: Lower frequency content, reflecting slower system dynamics crucial for detection.

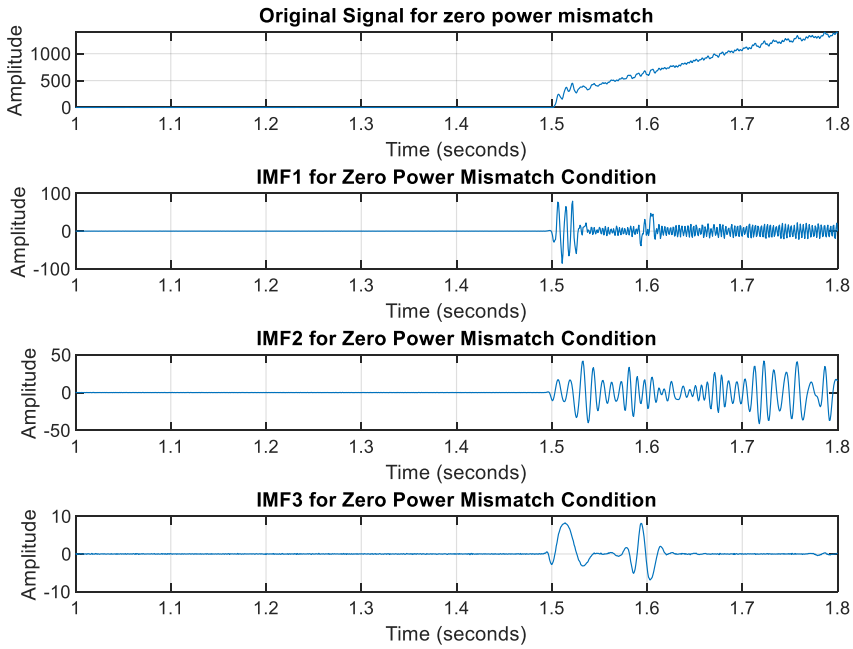

Fig. 5. Islanding case of Negative sequence voltage and IMFs during zero power mismatch

With a 50% power mismatch, larger voltage variations are observed (*Figure 6*), improving discrimination between islanding and non-islanding events. IMF1 captures fast transients, while IMF2 and IMF3 reflect slower dynamics, highlighting the impact of power mismatch on islanding detection.

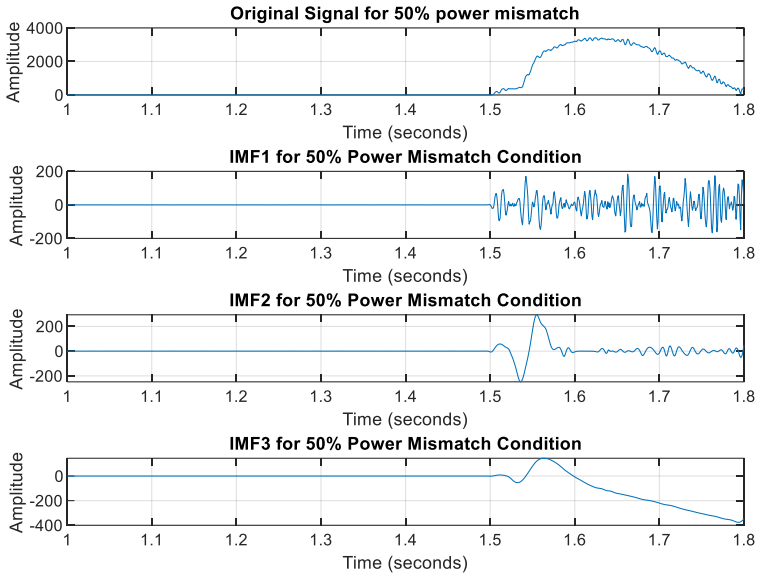

Fig. 6. Islanding case of negative sequence voltage and IMFs @50% power mismatch

3.3. Fault Scenario (C2)

Various faults, including single-phase, two-phase, and three-phase faults, were simulated at different distances from the PCC (5 km and 14 km). Resistance values ranged from 1 Ω to 70 Ω and were cleared after 300 ms.

Figures 7–9 illustrate negative sequence voltage responses for different fault types. Lower voltages at higher fault resistance complicate islanding detection.

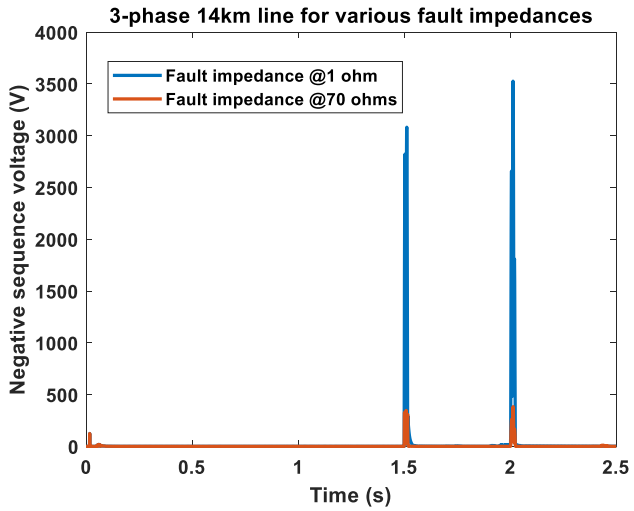

Fig. 7. 3-phase fault inception time 1.5 seconds negative sequence voltage waveform

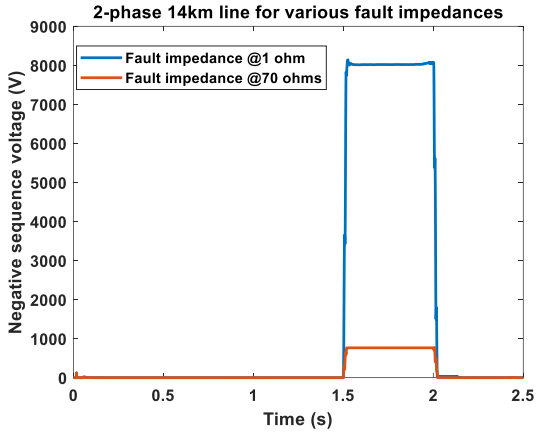

Fig. 8. 2-phase fault inception time 1.5 seconds negative sequence voltage waveform

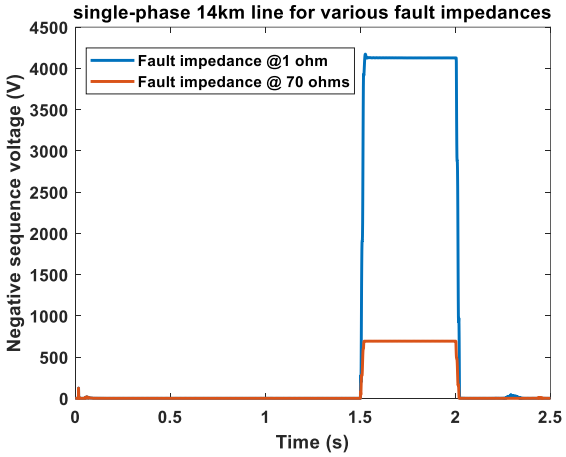

Fig. 9. 1-phase fault inception time 1.5 seconds negative sequence voltage waveform

CEEMDAN was applied to extract IMF features from the 1.5–1.8 s window around the fault event (*Figure 10*).

IMF1 captures high-frequency transient response while IMF2 & IMF3: Reveal lower-frequency components essential for distinguishing faults from islanding.

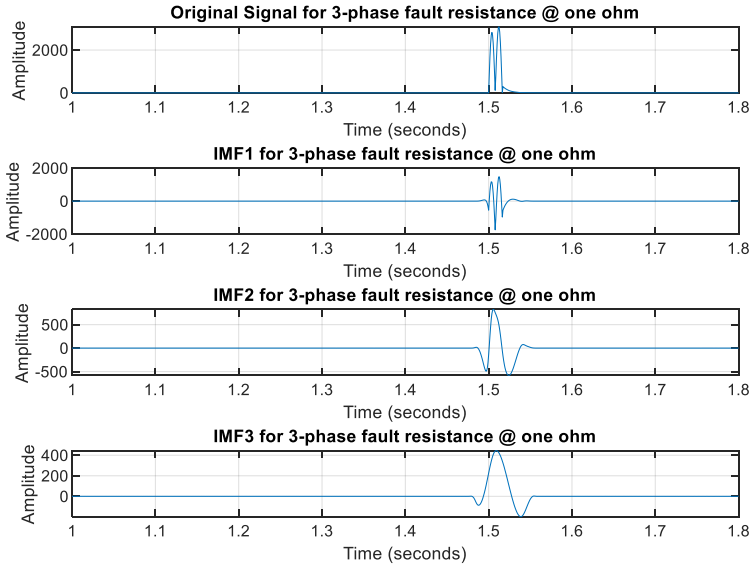

Fig. 10. 3-phase grid fault and IMFs for a fault resistance of one ohm

3.4. Load Switching Scenario (C3)

Load switching events were simulated at t = 1.5 s, with capacities ranging from 10 MW to 20 MW. *Figures 11–12* display voltage variations at the PCC for local and grid load switching.

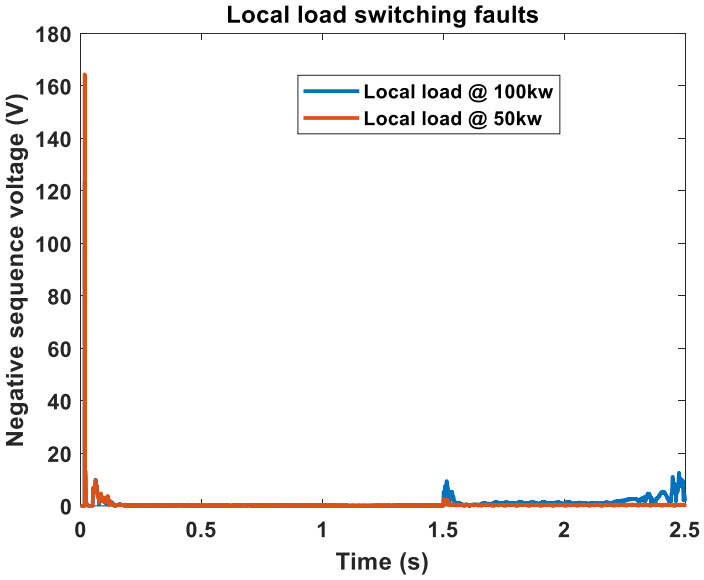

Fig. 11. Local load switching fault

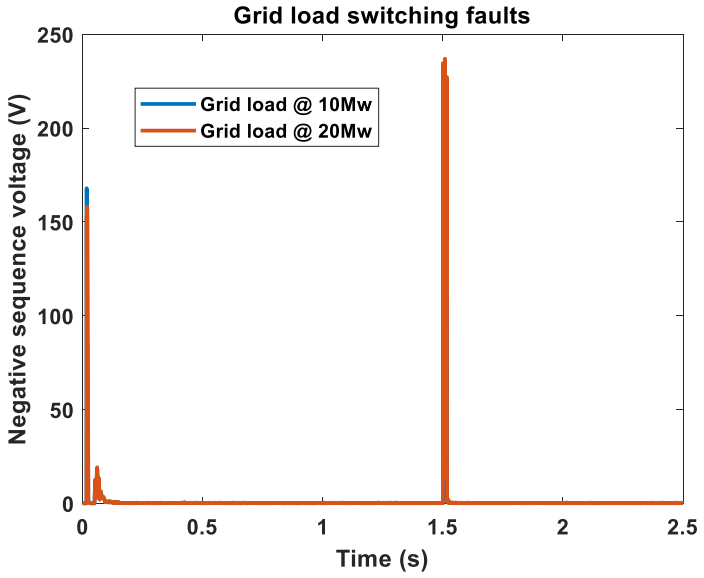

Fig. 12. Grid load switching fault

IMFs corresponding to different load magnitudes (*Figures 13–14*) demonstrate that larger load changes induce more significant negative sequence voltage variations, which are critical for detecting disturbances that could be misinterpreted as islanding.

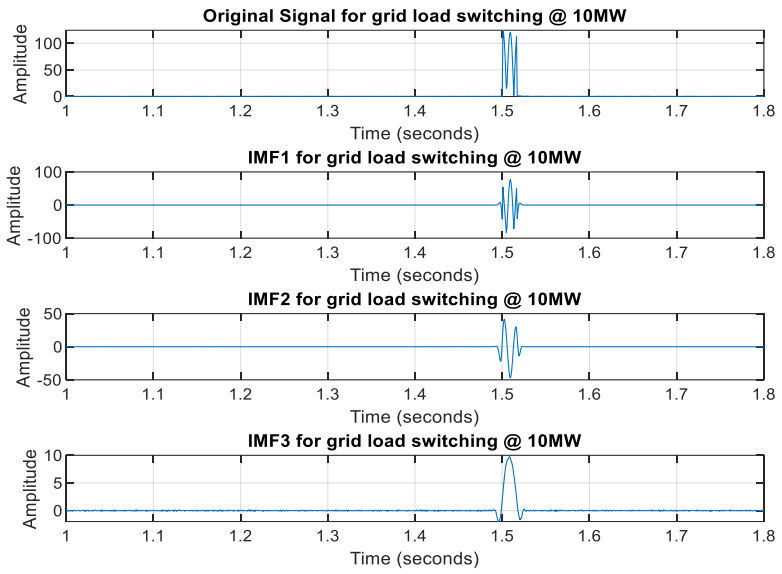

Fig. 13. Switching fault and IMFs for various loading effect(10MW)

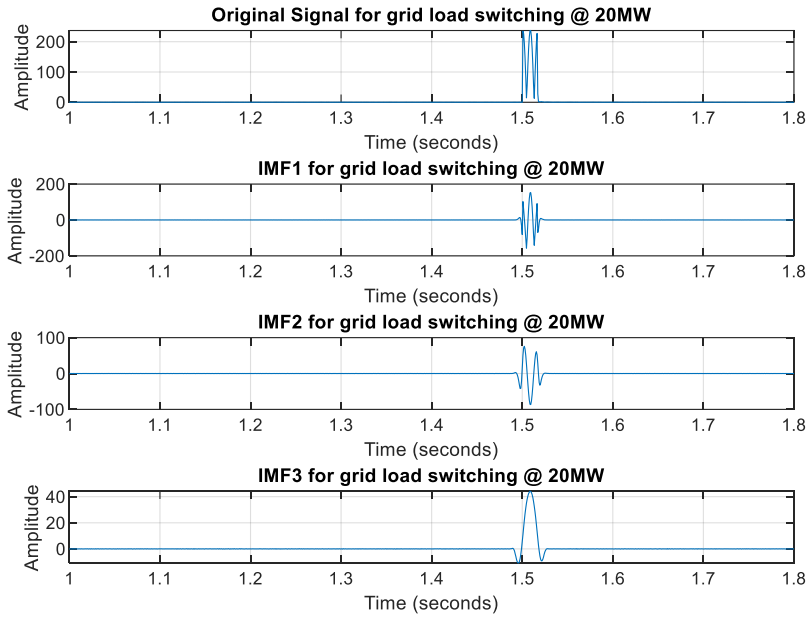

Fig. 14. Switching fault and IMFs for various loading effect(20MW)

3.5. Feature Analysis for Islanding Detection

Three statistical features were extracted from the IMFs for islanding detection: normalized maximum value, standard deviation, and entropy.

Normalized Max (*Figure 15*) has higher during islanding events, lower for non-islanding scenarios.

Normalized Standard Deviation (*Figure 16*) has larger deviations during islanding.

Normalized Entropy (*Figure 17*) has lower entropy in islanding conditions, higher in non-islanding events.

These features provided clear discrimination between islanding and non-islanding scenarios, forming the input for the PANN classifier.

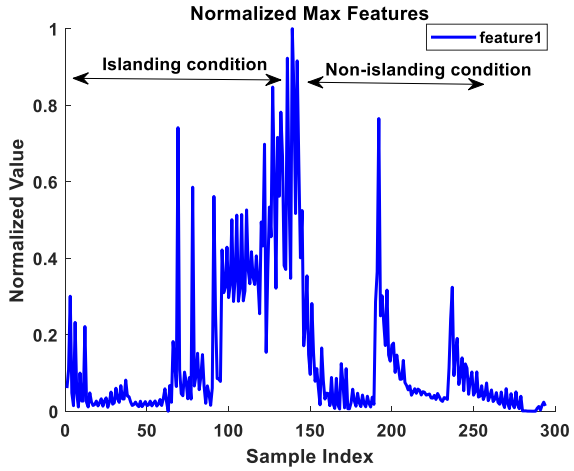

Fig. 15. Normalized max feature analysis

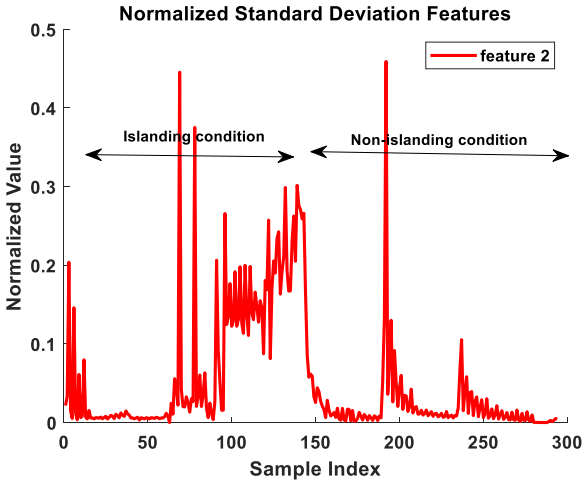

Fig. 16. Normalized std features analysis

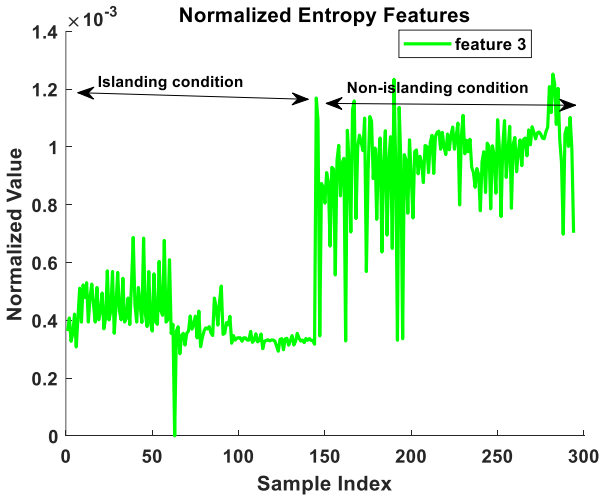

Fig. 17. Normalized entropy features analysis

3.6. PANN Training and Performance

The PANN with a single hidden layer of 3 neurons was trained over 24 iterations. Performance metrics included: Training accuracy: 96.4%, Validation accuracy: 97.1%, Testing accuracy: 100%, Overall accuracy: 97.0%.

Figure 18 shows regression performance, and *Figure 19* highlights cross-entropy loss reduction to 0.09399 at epoch 18, indicating effective feature learning and model convergence.

Training and testing times were 4109.85 ms and 18.97 ms, respectively, demonstrating real-time applicability.

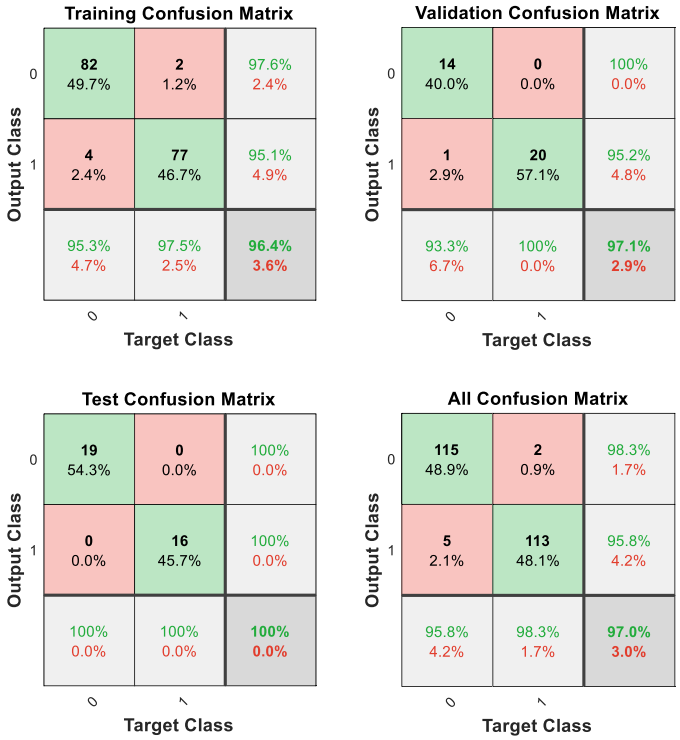

Fig. 18. Performance of CEEMDAM-PANN training with single hidden layer 3

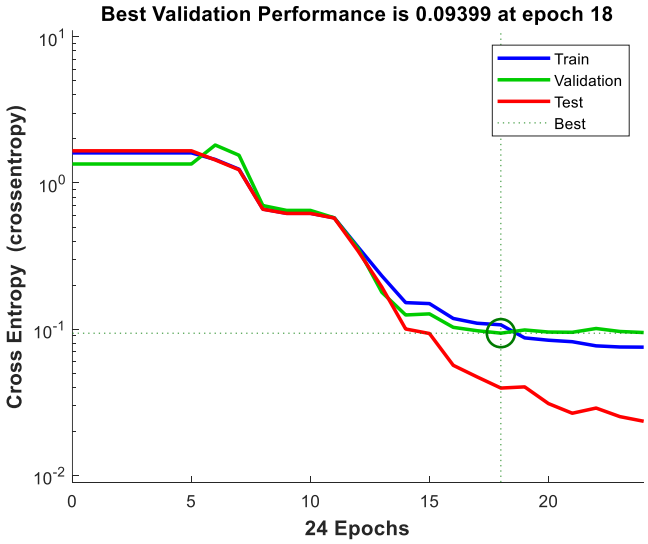

Fig. 19. Performance of CEEMDAN-PANN training with single hidden layers 3 neurons

3.7. 5-Fold Cross-Validation Performance

The model was evaluated using 5-fold cross-validation. *Figure 20* illustrates fold-wise training and testing accuracies. Table 4 summarizes performance metrics:

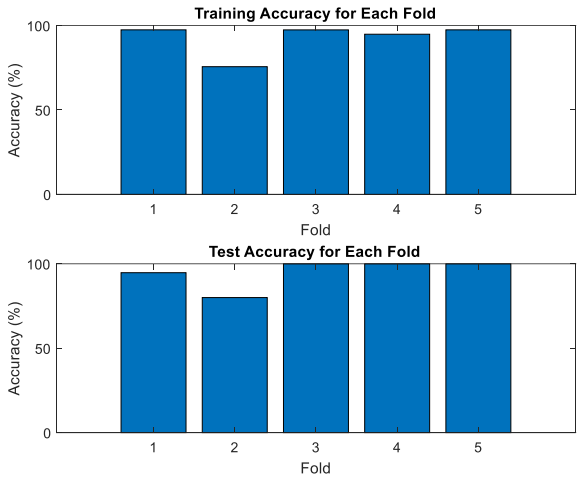

Fig. 19. Training and test accuracy of CEEMDAN-PANN on 5-fold cross validation

Table 2 cross validation Performance of the CEEMDAN-PANN islanding detection

Fold	Accuracy (%)	Precision	Recall	F1_score
1	94.83	0.97	0.93	0.95
2	98.61	1	0.97	0.98
3	94.92	0.97	0.93	0.95
4	96.61	0.97	0.97	0.97
5	98.31	1	0.97	0.98

These results indicate high robustness and generalization across different dataset subsets.

3.8. Classification Results

The CEEMDAN–PANN classifier achieved: 100% detection for islanding events and 96.67% detection for non-islanding events (Table 3, *Figure 21*).

Table 3 CEEMDAN-PANN classification result with IMFs

classes	No of cases	Correct detection	accuracy
Non-islanding	30	29	96.67
islanding	29	29	100

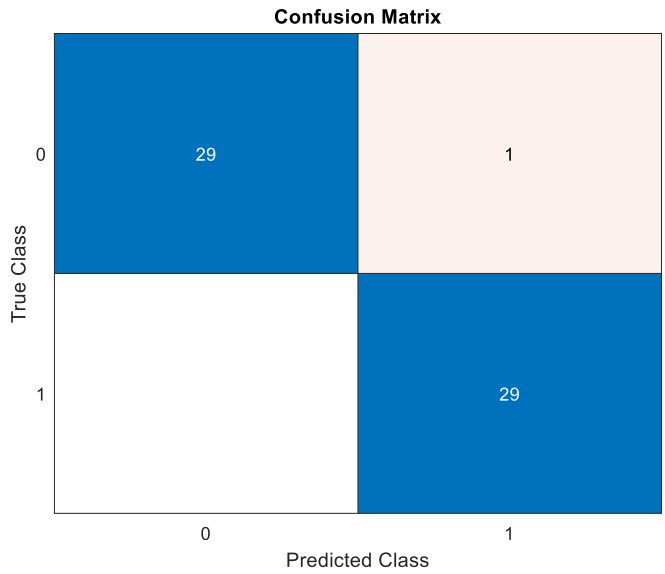

Fig. 20. CEEMDAN-PANN confusion matrix for islanding condition

3.9. Comparison with Existing Methods

The proposed method outperformed recent approaches in both accuracy and detection speed (Table 5):

Table 4 comparison with existing methods

Reference	**Signal processing**	**classifier**	**Accuracy (%)**
[19]	Wavelet transform	ANN	91.43
[20]	Wavelet transform	Decision tree	97.9
[21]	S-transform	KNN	98.1
[22]	Wavelet-singular spectrum entropy	Deep learning	98.4
Proposed method	CEEMDAN	Pattern artificial neural network	98.6

Detection time of 0.1806 seconds, suitable for real-time applications

4. CONCLUSION

This study presents a robust CEEMDAN–PANN-based islanding detection method for solar PV-distributed generation systems. By leveraging negative sequence voltage, selecting significant IMFs, and extracting max, standard deviation, and entropy features, the approach achieved high detection accuracy (98.6%) and fast response (0.1806 s).

Compared to conventional methods, the proposed framework reduces the non-detection zone and ensures reliable, real-time identification of islanding events under power mismatches, load switching, and noisy environments. Future work will focus on field implementation and optimization for evolving smart grid scenarios.

REFERENCES

[1] A. K. Hamid, N. T. Mbungu, A. Elnady, R. C. Bansal, A. A. Ismail, and M. A. AlShabi, "A systematic review of grid-connected photovoltaic and photovoltaic/thermal systems: Benefits, challenges and mitigation," *Energy Environ.*, vol. 34, no. 7, pp. 2775–2814, 2023, doi: 10.1177/0958305X221117617.

[2] S. K. G. Manikonda and D. N. Gaonkar, "Comprehensive review of IDMs in DG systems," *IET Smart Grid*, vol. 2, no. 1, pp. 11–24, 2019, doi: 10.1049/iet-stg.2018.0096.

[3] A. Serrano-Fontova, J. A. Martinez, P. Casals-Torrens, and R. Bosch, "A robust islanding detection method with zero-non-detection zone for distribution systems with DG," *Int. J. Electr. Power Energy Syst.*, vol. 133, p. 107247, 2021, doi: 10.1016/j.ijepes.2021.107247.

[4] P. Systems, "IEEE standards," *IEEE Spectr.*, vol. 13, no. 5, pp. 108–108, 2013, doi: 10.1109/mspec.1976.6369202.

[5] R. Bakhshi-Jafarabadi, J. Sadeh, A. Serrano-Fontova, and E. Rakhshani, "Review on islanding detection methods for grid-connected photovoltaic systems, existing limitations and future insights," *IET Renew. Power Gener.*, vol. 16, no. 15, pp. 3406–3421, 2022, doi: 10.1049/rpg2.12554.

[6] S. Perlenfein, M. Ropp, J. Neely, S. Gonzalez, and L. Rashkin, "Subharmonic power line carrier (PLC) based island detection," *Conf. Proc. - IEEE Appl. Power Electron. Conf. Expo. - APEC*, vol. 2015-May, no. May, pp. 2230–2236, 2015, doi: 10.1109/APEC.2015.7104659.

[7] O. Tshenyego, R. Samikannu, and B. Mtengi, "Wide area monitoring, protection, and control application in islanding detection for grid integrated distributed generation: A review," *Meas. Control (United Kingdom)*, vol. 54, no. 5–6, pp. 585–617, 2021, doi: 10.1177/0020294021989768.

[8] N. Gupta, R. Dogra, R. Garg, and P. Kumar, "Review of islanding detection schemes for utility interactive solar photovoltaic systems," *Int. J. Green Energy*, vol. 19, no. 3, pp. 242–253, 2022, doi: 10.1080/15435075.2021.1941048.

[9] N. A. Larik, M. F. Tahir, Z. M. S. Elbarbary, M. Z. Yousaf, and M. A. Khan, "A comprehensive literature review of conventional and modern islanding detection methods," *Energy Strateg. Rev.*, vol. 44, no. November, p. 101007, 2022, doi: 10.1016/j.esr.2022.101007.

[10] M. S. Thomas and P. P. Terang, "Islanding detection using decision tree approach," *2010 Jt. Int. Conf. Power Electron. Drives Energy Syst. PEDES 2010 2010 Power India*, pp. 1–6, 2010, doi: 10.1109/PEDES.2010.5712394.

[11] A. Ezzat, B. E. Elnaghi, and A. A. Abdelsalam, "Microgrids islanding detection using Fourier transform and machine learning algorithm," *Electr. Power Syst. Res.*, vol. 196, no. February, p. 107224, 2021, doi: 10.1016/j.epsr.2021.107224.

[12] P. K. Dash, M. Padhee, and T. K. Panigrahi, "Electrical Power and Energy Systems A hybrid time – frequency approach based fuzzy logic system for power island detection in grid connected distributed generation," *Int. J. Electr. Power Energy Syst.*, vol. 42, no. 1, pp. 453–464, 2012, doi: 10.1016/j.ijepes.2012.04.003.

[13] Himanshu Jyoti Saikia, "Development of a Passive Islanding Detection Method based Fuzzy Controller for a Grid Connected Distributed Generator.," *Int. J. Eng. Res.*, vol. V5, no. 12, pp. 308–311, 2016, doi: 10.17577/ijertv5is120242.

[14] M. I. Dieste-Velasco, "Application of a pattern-recognition neural network for detecting analog electronic circuit faults," *Mathematics*, vol. 9, no. 24, 2021, doi: 10.3390/math9243247.

[15] S. Kujabi, E. A. Frimpong, and F. B. Effah, "Energy-Efficient Islanding Detection Using CEEMDAN and Neural Network Integration in Photovoltaic Distribution System." [Online]. Available: https://www.ijeca.info

[16] L. Zhao, Z. Li, J. Zhang, and B. Teng, "An Integrated Complete Ensemble Empirical Mode Decomposition with Adaptive Noise to Optimize LSTM for Significant Wave Height Forecasting," *J. Mar. Sci. Eng.*, vol. 11, no. 2, 2023, doi: 10.3390/jmse11020435.

[17] S. Paul, "Islanding Detection in Grid-Connected 100 KW Photovoltaic System Using Wavelet Transform," *Int. J. Innov. Res. Sci. Eng. Technol.*, vol. 5, no. 5, pp. 92–98, 2016.

[18] P. Jaiswal, S. K. Srivastava, and K. B. Sahay, "Modeling and simulation of proposed 100 KW solar PV array power plant for MMMUT Gorakhpur," *Int. Conf. Emerg. Trends Electr. Electron. Sustain. Energy Syst. ICETEESES 2016*, pp. 261–266, 2016, doi: 10.1109/ICETEESES.2016.7581391.

[19] Z. Guan and Y. Liao, "A New islanding detection method based on wavelet-Transform and ann for micro-grid including inverter assisted distributed generator," *Int. J. Emerg. Electr. Power Syst.*, vol. 20, no. 5, pp. 1–10, 2019, doi: 10.1515/ijeeps-2019-0074.

[20] M. A. Khan, A. Haque, and V. S. B. Kurukuru, "Machine Learning Based Islanding Detection for Grid Connected Photovoltaic System," *2019 Int. Conf. Power Electron. Control Autom. ICPECA 2019 - Proc.*, vol. 2019-Novem, no. 1, 2019, doi: 10.1109/ICPECA47973.2019.8975614.

[21] M. Mishra, C. K. Patra, P. K. Muni, D. A. Gadanayak, and T. Parida, "Islanding detection in distributed generation system based on optimized KNN utilizing S-transform based features," *2023 Int. Conf. Adv. Power, Signal, Inf. Technol.*, pp. 41–47, 2023, doi: 10.1109/APSIT58554.2023.10201758.

[22] X. Kong, X. Xu, Z. Yan, S. Chen, H. Yang, and D. Han, "Deep learning hybrid method for islanding detection in distributed generation," *Appl. Energy*, vol. 210, no. August 2017, pp. 776–785, 2018, doi: 10.1016/j.apenergy.2017.08.014.